International Journal of Non-Linear Mechanics 75 (2015) 59–66

Contents lists available at ScienceDirect

International Journal of Non-Linear Mechanics

journal homepage: www.elsevier.com/locate/nlm

Coiling of an elastic beam inside a disk: A model for spider-capture silk

Hervé Elettro [a,b], Fritz Vollrath [c], Arnaud Antkowiak [a,b], Sébastien Neukirch [a,b,*]

[a] Centre National de la Recherche Scientifique, UMR 7190, Institut Jean Le Rond d'Alembert, F-75005 Paris, France
[b] Sorbonne Universités, UPMC Univ Paris 06, UMR 7190, Institut Jean Le Rond d'Alembert, F-75005 Paris, France
[c] Oxford Silk Group, Zoology Department, University of Oxford, UK

ARTICLE INFO

Article history:
Received 3 February 2015
Received in revised form
20 March 2015
Accepted 22 March 2015
Available online 30 March 2015

Keywords:
Coiling
Post-buckling
Elastica
Equilibria paths
Continuation
Stability

ABSTRACT

Motivated by recent experimental observations of capillary-induced spooling of fibers inside droplets both in spider capture silk and in synthetic systems, we investigate the behavior of a fiber packed in a drop. Using a simplified 2D model, we provide analytical predictions for the buckling threshold and the deep post-buckling asymptotic behavior. The threshold for spooling is found to be in particularly good agreement with experimental results. We further solve the Elastica equations for a fiber confined in a soft potential, and track the equilibrium paths using numerical continuation techniques. A wealth of different paths corresponding to different symmetries is uncovered, and their stability is finally discussed.

1. Introduction

The mechanical properties of spider silk are often presented as outstanding [1,2]. An indeed, most silk threads outperform the best man-made fibers, such a Kevlar, at least in terms of toughness [3]. To a large extent, these properties rely on the molecular architecture of the silk. For example, it has been shown that the building blocks of flagelliform silk involve molecular nanosprings [4]. In 1989 however, a team comprising a zoologist and a physicist reported on coiling and packing of the core filament inside a glue droplet [5]. This *windlass mechanism*, as it was called, provided indirect evidence that the glue droplets may as well play a role in the mechanical response of the silk thread. These results have been a subject of debate in the community, and it is only very recently that the mechanism has been observed to be active in a real spider web, see Fig. 1 (left) [6]. A natural question that arises in this context is the role played by the molecular structure of the silk and the glue in the observed coiling. An experimental answer to this question is provided in Fig. 1 (right), where a micron-sized artificial thread bearing a silicon oil droplet also exhibits the coiling mechanism and packing behavior, therefore demonstrating that capillarity and elasticity are sufficient ingredients to explain the mechanism.

Interestingly, the shape adopted by the filament inside the drop can be as different as a perfectly ordered closely packed annular bundle or a completely disordered tangle. This behavior is reminiscent of the organization of packed wires in rigid [7] and elastic [8] spherical shells, patterns of folded structures such as plant leaves or crumpled paper [9,10], and DNA packing inside capsids [11–13]. The purpose of the present paper is to explore theoretically in a simplified setting the shape and stability of strongly post-buckled states in order to lay down the basis for a deeper understanding of the windlass mechanism.

The paper is organized as follows. In Section 2 we present the problem and the equilibrium equations. In Section 3 we perform a linear stability analysis of the straight beam and predict the buckling threshold. Experimental results are confronted to theoretical in Section 4. Finally, we describe the non-linear response of the system in terms of equilibrium solutions and their stability in Section 5.

2. Model

We consider an elastic beam in interaction with a liquid disk and under the action of a tensile end-load. As indicated in Fig. 2, we restrict to planar deformations of the beam, X and Y denoting the horizontal and vertical directions respectively. The beam has length L and a circular cross-section of radius h. We work under the slender ($L \gg h$) Euler–Bernoulli hypotheses where the beam is considered inextensible and unshearable. Configurations are thus fully described by the position and orientation of the centerline. We use the arc-length $S \in [0, L]$ and note $\theta(S)$ the angle between the tangent of the beam and the horizontal. The presence of the liquid disk generates capillary forces due to the contrast of surface energy, the interaction

* Corresponding author.
E-mail address: sebastien.neukirch@upmc.fr (S. Neukirch).

http://dx.doi.org/10.1016/j.ijnonlinmec.2015.03.008
0020-7462/

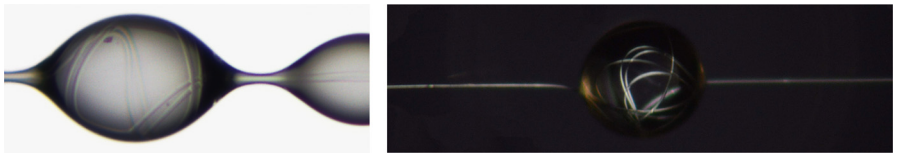

Fig. 1. Experiments on fibers bent inside liquid drops. *Left*: microscopic photograph of spider capture silk. Flagelliform core filaments are seen to be coiled and packed inside a (typically 300μ wide) glue droplet. *Right*: same mechanism reproduced artificially with a 200 μm synthetic droplet and fiber (see experimental verification section in Section 4). Reproduced from [6].

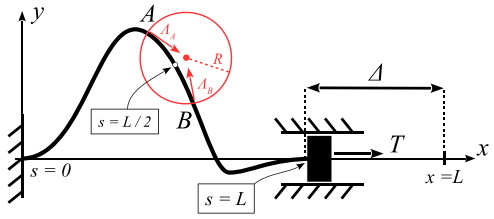

Fig. 2. An elastic beam held in tension at its extremities, and buckling under the action of compressive forces at a disk. The beam is clamped at both ends. The deformation of the beam is described by the angle $\theta(S)$ between the tangent to the beam and the x-axis, where $S \in [0, L]$ is the arc-length along the beam.

energy of the beam with the liquid being smaller than the interaction energy of the beam with the air. Capillary forces are two-fold: (i) meniscus forces applied on the beam at the entrance and exit of the disk, and (ii) barrier forces that prevent the beam from exiting the disk elsewhere than at the meniscus points. We consider that the drop is undeformable and thus remains a disk throughout the experiments. As shown in Appendix A, meniscus forces are pointing toward the center of the disk (see Eqs. (A.15) and (A.18)) and their intensity is related to the angle between their direction and the tangent to the beam at the meniscus points (see Eq. (A.25)). A soft-wall barrier potential [14]

$$V(X,Y) = \frac{V_0}{1+\rho-(1/R)\sqrt{(X-X_C)^2+(Y-Y_C)^2}} \tag{1}$$

is used to retain the beam inside the disk, centered on (X_C, Y_C) and of radius R. The small dimensionless parameter ρ is introduced to avoid the potential to diverge at the meniscus points A and B, where the rod enters and exits the disk. The intensity V_0 of the potential is chosen to be small, the hard-wall limit being $V_0 \to 0$. Kinematics, relating the position (X,Y) of the rod and the inclination $\theta$of its tangent $(\cos\theta, \sin\theta)$ with the horizontal, the bending constitutive relation, relating the curvature $\theta'(S)$ to the moment $M(S)$, and finally force (N_x, N_y) and moment balance are detailed in Appendix A and read

$$X'(S) = \cos\theta, \quad Y'(S) = \sin\theta \tag{2a}$$

$$EI\theta'(S) = M, \quad M'(S) = N_x \sin\theta - N_y \cos\theta \tag{2b}$$

$$N_x'(S) = \chi\frac{\partial V}{\partial X} + \delta(S-S_A)\Lambda_A\frac{X_A-X_C}{R} + \delta(S-S_B)\Lambda_B\frac{X_B-X_C}{R} \tag{2c}$$

$$N_y'(S) = \chi\frac{\partial V}{\partial Y} + \delta(S-S_A)\Lambda_A\frac{Y_A-Y_C}{R} + \delta(S-S_B)\Lambda_B\frac{Y_B-Y_C}{R} \tag{2d}$$

where S is the arc-length along the rod, and $(\,)' = \mathrm{d}(\,)/\mathrm{d}S$. We define the coordinates of point A as $(X_A, Y_A) = (X(S_A), Y(S_A))$, same for point B. Note that the potential V has the dimension of an energy per unit of arc-length of the beam. For $S \in [S_A; S_B]$ the rod lies inside the disk and we have $\chi = 1$, otherwise $\chi = 0$. The Dirac distribution $\delta(S)$ localizes meniscus forces at points A and B. The rod material has Young's modulus E and the second moment of area $I = \pi h^4/4$. The intensities Λ_A and Λ_B of the meniscus forces are unknown but related to surface tension γ_{LV} through Eq. (A.25), where $F_\gamma = 2\pi h\gamma_{LV}\cos\alpha_Y$ with α_Y being the Young–Dupré wetting angle ($\gamma_{SV} - \gamma_{SL} = \gamma_{LV}\cos\alpha_Y$), and where $V_A = V_B = V_0/\rho$ are small compared to F_γ. We restrict ourself to cases where the disk is centered on the mid-point of the rod, that is we introduce Σ such that $S_A = L/2 - \Sigma$ and $S_B = L/2 + \Sigma$. The rod has then 2Σ of its arc-length spent inside the disk. Finally the external applied tension is noted $T = N_x(L)$.

2.1. Non-dimensionalization

We use the diameter $D = 2R$ of the disk as unit length, and the buckling load EI/D^2 as unit force. We thus introduce the following dimensionless quantities:

$$s = \frac{S}{D}; \quad \sigma = \frac{\Sigma}{D}; \quad \ell = \frac{L}{D}; \quad (x,y) = \frac{(X,Y)}{D}; \quad n = \frac{ND^2}{EI}; \quad t = \frac{TD^2}{EI} \tag{3a}$$

$$f_\gamma = \frac{F_\gamma D^2}{EI}; \quad m = \frac{MD}{EI}; \quad \lambda_{A,B} = \frac{\Lambda_{A,B}D^2}{EI}; \quad (v, v_0) = \frac{(V, V_0)D^2}{EI} \tag{3b}$$

and $\delta(s) = D\delta(S)$. We then have

$$v(x,y) = v_0\left(1+\rho-2\sqrt{(x-x_C)^2+(y-y_C)^2}\right)^{-1} \text{ and}$$

$$x'(s) = \cos\theta, \quad y'(s) = \sin\theta \tag{4a}$$

$$\theta'(s) = m, \quad m'(s) = n_x\sin\theta - n_y\cos\theta \tag{4b}$$

$$n_x'(s) = \chi\frac{\partial v}{\partial x} + 2\delta(s-s_A)\lambda_A(x_A-x_C) + 2\delta(s-s_B)\lambda_B(x_B-x_C) \tag{4c}$$

$$n_y'(s) = \chi\frac{\partial v}{\partial y} + 2\delta(s-s_A)\lambda_A(y_A-y_C) + 2\delta(s-s_B)\lambda_B(y_B-y_C) \tag{4d}$$

where $(\,)' = \mathrm{d}(\,)/\mathrm{d}s$, and $s_A = \ell/2 - \sigma$, $s_B = \ell/2 + \sigma$.

2.2. Boundary-value problem

We consider v_0, ρ, f_γ, and ℓ as fixed parameters and we look for equilibrium solutions by integrating (4) with the initial conditions

$$x(0) = 0; \quad y(0) = 0; \quad \theta(0) = 0; \quad m(0) = m_0; \quad n_x(0) = n_{x0};$$

$$n_y(0) = n_{y0} \tag{5}$$

where m_0, n_{x0}, and n_{y0} are unknowns to be accompanied with σ, x_C, y_C, λ_A, and λ_B. We therefore have eight unknowns which are balanced by the following seven conditions. At the $s = \ell$ end of the rod, clamped boundary conditions read

$$y(\ell) = 0; \quad \theta(\ell) = 0 \tag{6}$$

The requirement that points A and B lie on the circle yields the conditions

$$[x_A - x_C]^2 + [y_A - y_C]^2 = 1/4; \quad [x_B - x_C]^2 + [y_B - y_C]^2 = 1/4 \tag{7}$$